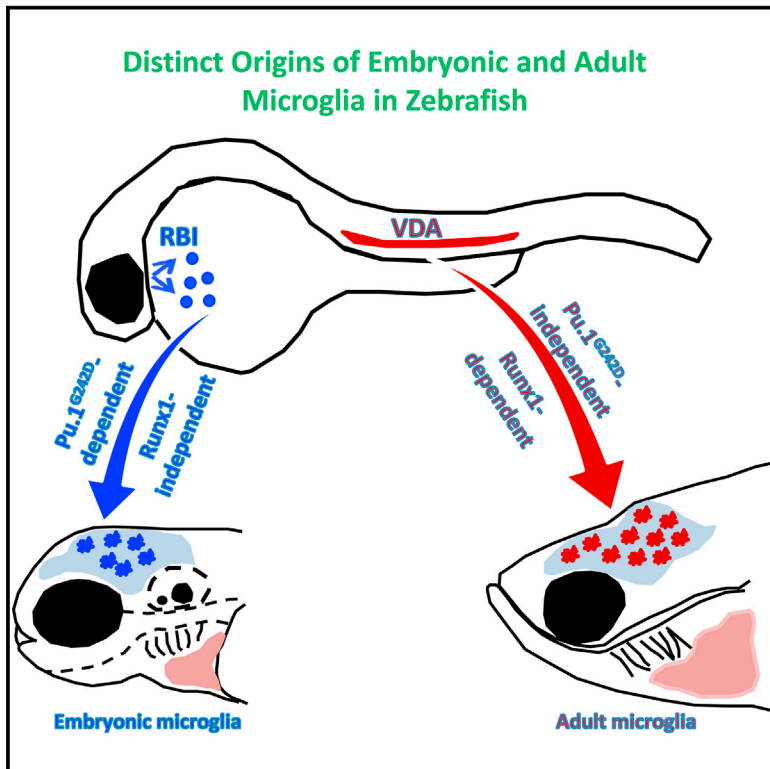


# Developmental Cell

## Temporal-Spatial Resolution Fate Mapping Reveals Distinct Origins for Embryonic and Adult Microglia in Zebrafish

### Graphical Abstract



### Authors

Jin Xu, Lu Zhu, Sicong He, ..., Tao Yu, Jianan Y. Qu, Zilong Wen

### Correspondence

eequ@ust.hk (J.Y.Q.),  
zilong@ust.hk (Z.W.)

### In Brief

Microglia are tissue-resident macrophages that reside in the brain, spinal cord, and retina. Using light-induced temporal-spatial resolution fate mapping, Xu and Zhu et al. show that two distinct sources, the rostral blood island and ventral wall of dorsal aorta, give rise to microglia possessing different genetic program and colonization potential in zebrafish.

### Highlights

- Embryonic microglia in zebrafish initiate from the rostral blood island
- Adult microglia in zebrafish arise from the ventral wall of dorsal aorta
- The RBI- and VDA-derived microglia are differentially regulated by Pu.1
- The VDA-derived microglia are Runx1 dependent but cMyb independent

# Temporal-Spatial Resolution Fate Mapping Reveals Distinct Origins for Embryonic and Adult Microglia in Zebrafish

Jin Xu,<sup>1,3</sup> Lu Zhu,<sup>1,3</sup> Sicong He,<sup>2</sup> Yi Wu,<sup>1</sup> Wan Jin,<sup>1</sup> Tao Yu,<sup>1</sup> Jianan Y. Qu,<sup>2,\*</sup> and Zilong Wen<sup>1,\*</sup>

<sup>1</sup>Division of Life Science, State Key Laboratory of Molecular Neuroscience

<sup>2</sup>Department of Electronic and Computer Engineering

Center of Systems Biology and Human Health, Hong Kong University of Science and Technology, Clear Water Bay, Kowloon, Hong Kong, PRC

<sup>3</sup>Co-first author

\*Correspondence: [eequ@ust.hk](mailto:eequ@ust.hk) (J.Y.Q.), [zilong@ust.hk](mailto:zilong@ust.hk) (Z.W.)

<http://dx.doi.org/10.1016/j.devcel.2015.08.018>

## SUMMARY

Microglia are CNS resident macrophages, and they play important roles in neural development and function. Recent studies have suggested that murine microglia arise from a single source, the yolk sac (YS), yet these studies lack spatial resolution to define the bona fide source(s) for microglia. Here, using light-induced high temporal-spatial resolution fate mapping, we challenge this single-source view by showing that microglia in zebrafish arise from multiple sources. The embryonic/larval microglia originate from the rostral blood island (RBI) region, the equivalent of mouse YS for myelopoiesis, whereas the adult microglia arise from the ventral wall of dorsal aorta (VDA) region, a tissue also producing definitive hematopoiesis in mouse. We further show that the VDA-region-derived microglia are *Runx1* dependent, but *cMyb* independent, and developmentally regulated differently from the RBI region-derived microglia. Our study establishes a new paradigm for investigating the development and function of distinct microglia populations.

## INTRODUCTION

Microglia are macrophages that reside in the brain, spinal cord, and retina (Prinz and Priller, 2014). Microglia have been thought to mainly function as primary immune effector cells to remove infectious agents, plaques, and damaged/apoptotic cells (Kreutzberg, 1995). However, growing evidence has suggested that microglia also play critical roles in the regulation of neurogenesis and neural functions (Salter and Beggs, 2014). The importance of microglia in the CNS is further elucidated by the observations that irregularities in microglia are known to associate with the onset and development of various neurodegenerative diseases (Prinz and Priller, 2014; Salter and Beggs, 2014). Thus, a comprehensive fate mapping of microglia origin will be essential for our understanding of the development and function of microglia in the developing and adult CNS.

In the past decade, a series of lineage tracing studies have been carried out to dissect the origin of microglia (Epelman et al., 2014; Ginhoux et al., 2010; Gomez Perdiguero et al., 2015; Hashimoto et al., 2013; Hoeffel et al., 2015; Kierdorf et al., 2013; Perdiguero et al., 2014; Schulz et al., 2012). The current prevailing view is that microglia are derived from one single source, the yolk sac (YS) in mice. This view is mainly based on two recent studies (Ginhoux et al., 2010; Schulz et al., 2012), in which the investigators utilized the *Runx1* and colony-stimulating factor 1 receptor (*Csf1r*) promoter-controlled CreER-*loxP* system to track the fates of *Runx1*-expressing (*Runx1*<sup>+</sup>) and *Csf1r*-expressing (*Csf1r*<sup>+</sup>) cells from embryonic day (E) 6.5 to E10.5. The results suggested that the majority of microglia in adult mouse brain seemed to be derived from the *Runx1*<sup>+</sup> or *Csf1r*<sup>+</sup> cells that emerged before E8–8.5. Given the fact that murine primitive hematopoiesis occurs in the YS between E7 and E8.5 and the definitive hematopoiesis emerges in the aorta, gonads, and mesonephros (AGM) from E9.5 to E10.5 (Lichanska and Hume, 2000; Orkin and Zon, 2008), the authors concluded that microglia in mice originate from the primitive hematopoietic precursor cells born in the YS. However, the promoter-controlled CreER-*loxP* tracking system used in these fate mapping studies does not provide sufficient spatial resolution to resolve the origin of microglia unambiguously. For example, studies have indicated that hematopoietic activity can be detected in the AGM prior to the appearance of the definitive hematopoietic stem cells (HSCs) (Lin et al., 2014). Moreover, other hematopoietic compartments including the placenta and head endothelium in mid-gestation mouse embryo also contain substantial hematopoietic activity (Gekas et al., 2005; Li et al., 2012b; Ottersbach and Dzierzak, 2005). Upon tamoxifen induction, the hematopoietic cells in these compartments might be labeled undesirably, potentially confounding the isolation of bona fide source(s) for microglia. Thus, a fate-mapping analysis with high temporal-spatial resolution is required to clarify the precise source of microglia.

Studies in the past decades have shown that similar to that in mammals, zebrafish experience successive waves of hematopoiesis and produce analogous mature blood cells (Jagannathan-Bogdan and Zon, 2013; Jing and Zon, 2011; Stachura and Traver, 2011; Xu et al., 2012). In zebrafish, the first or primitive wave of hematopoiesis initiates at ~11 hr post-fertilization

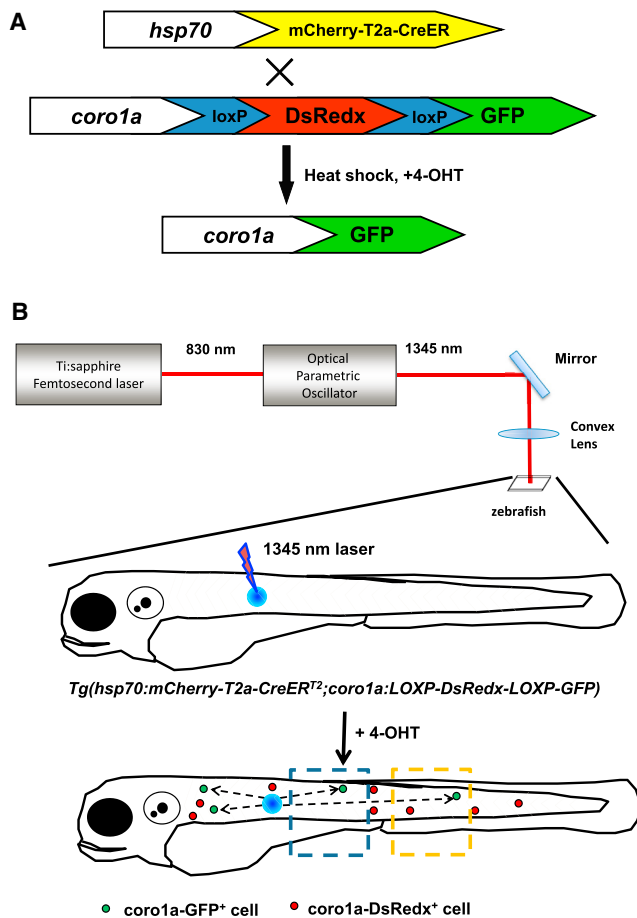


**Figure 1. A Schematic View of the IR-LEGO-CreER-loxP Cell Labeling System**

(A) The *Tg(coro1a:loxP-DsRedx-loxP-GFP)* reporter line outcrosses with the heat-shock-induced *CreER<sup>T2</sup>* transgenic fish *Tg(hsp70:mCherry-T2a-CreER<sup>T2</sup>)* to create *Tg(hsp70:mCherry-T2a-CreER<sup>T2</sup>; coro1a:loxP-DsRedx-loxP-GFP)* double transgenic fish, in which macrophages express *DsRedx* under normal condition but switch to *GFP* upon heat-shock-evoked *CreER*-mediated recombination of *loxP* sites.

(B) A femtosecond Ti:sapphire laser is tuned at 830 nm to pump an optical parametric oscillator to emit infrared beam with a wavelength of 1,345 nm. The 1,345 nm laser is then focused on the selected tissue of a desired developmental stage *Tg(hsp70:mCherry-T2a-CreER<sup>T2</sup>; coro1a:loxP-DsRedx-loxP-GFP)* transgenic fish by a coated convex lens to generate spatial-restricted heat shock, which induces local expression of *CreER*. Upon 4-OHT treatment, the *CreER*-mediated recombination of *loxP* sites occurs, leading to the induction of *GFP* expression in the macrophages derived from the heat-shocked region. The blue and orange dashed boxes indicate middle trunk and tail regions imaged in Figure 2B.

(hpf) from two distinctive regions: the posterior lateral mesoderm (PLM) and the rostral blood island (RBI). Similar to mammalian primitive hematopoiesis born in the YS, the PLM gives rise to embryonic erythrocytes critical for the survival of developing embryos and the RBI produces myeloid cells that contribute to the earliest macrophages and neutrophils in the circulation and tissues. The second or definitive wave of hematopoiesis originates from the ventral wall of dorsal aorta (VDA) at ~26–28 hpf and it produces HSCs capable of giving rise to all mature blood cells during fetal life and adulthood. In addition, a third or inter-

mediate wave of hematopoiesis has been identified to arise from a population of cells named committed erythromyeloid progenitors (EMPs), which are produced autonomously from the posterior blood island (PBI) at ~30 hpf (Bertrand et al., 2007). Similar to the case in mammals (Bertrand et al., 2005b), the intermediate hematopoiesis is transient and produces mainly myeloid and erythroid cells. The highly conserved hematopoietic program and the advantage of in vivo imaging and genetic amenability have made zebrafish an ideal model organism for studying the fate and development of microglia.

In this study, we used a high temporal-spatial resolution fate mapping approach to investigate the origin of microglia in zebrafish. We showed that microglia in developing and adult zebrafish brain, spinal cord, and retina arise from two different sources, in contrary to the single origin view. The embryonic/larval microglia in developing zebrafish brain and retina were derived from the RBI, the zebrafish counterpart of mouse YS for myelopoiesis, whereas the adult microglia arose from the VDA region, a tissue also producing definitive hematopoiesis in mouse. Genetic analysis revealed *pu.1* is differentially required for RBI- and VDA-region-derived microglia. Further study showed that the development of VDA-region-derived microglia is independent of *cmyb*, but requires *runx1* function.

## RESULTS

### The IR-LEGO-CreER-loxP System Provides High Temporal-Spatial Resolution Cell Labeling in Zebrafish

To set up a temporally and spatially restricted cell labeling, we generated a reporter line *Tg(coro1a:loxP-DsRedx-loxP-GFP)* in which leukocytes including microglia express *DsRedx* under normal conditions but switch to *GFP* upon *CreER*-mediated excision. The reporter line was outcrossed with the heat shock-inducible *Tg(hsp70:mCherry-T2a-CreER<sup>T2</sup>)* zebrafish (Hans et al., 2011). The resulting double transgenic line *Tg(hsp70:mCherry-T2a-CreER<sup>T2</sup>; coro1a:loxP-DsRedx-loxP-GFP)* was used for microglia fate mapping analysis (Figure 1A). To achieve the temporal-spatial restricted cell labeling, we applied the infrared laser-evoked gene operator (IR-LEGO) microscope heating system (Deguchi et al., 2009; Kamei et al., 2009), to induce *CreER<sup>T2</sup>* expression in a defined anatomy region at desired developmental stages by using the 1,345 nm infrared laser irradiation followed by 4-OH tamoxifen (4-OHT)-mediated activation of *CreER<sup>T2</sup>* (Figure 1B).

To confirm that the IR-LEGO-CreER-loxP system could indeed provide a temporal-spatial restricted cell labeling with high efficiency and specificity in vivo, we focused on the RBI, VDA, and PBI, three well-known zebrafish hematopoietic tissues capable of giving rise to myeloid cells (Ciau-Uitz et al., 2014; Xu et al., 2012). The RBI, VDA, and PBI regions of double transgenic *Tg(hsp70:mCherry-T2a-CreER<sup>T2</sup>; coro1a:loxP-DsRedx-loxP-GFP)* embryos were heat-shocked (two to four shots for each region; each shot spot is ~10 μm diameter in the focal plane and is irradiated for 2 min) by the 1,345 nm infrared laser at 12–16 hpf, 28–30 hpf, and 20–22 hpf, respectively. We chose these time windows because primitive myeloid precursors are restricted in the RBI region at 12–16 hpf, VDA endothelial hematopoietic transition occurs at 30 hpf, and the PBI region at 20–22 hpf is devoid of the RBI- and

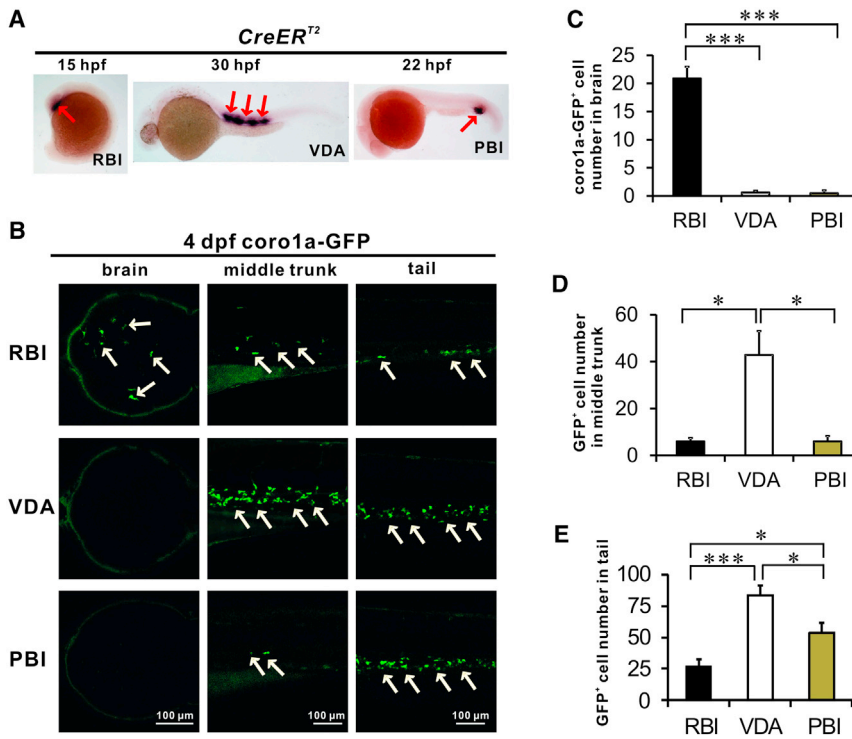


**Figure 2. The IR-LEGO-CreER-loxP System Provides a High Temporal-Spatial Resolution Labeling in Zebrafish RBI, VDA, and PBI Regions**

(A) Overexposed WISH staining shows that local 1,345 nm laser irradiation induces *CreER<sup>T2</sup>* expression in the RBI, VDA, and PBI regions. Red arrows indicate the overexposed *CreER<sup>T2</sup>* staining. (B) The distribution of the RBI-, VDA-region-, or PBI-derived cells (*coro1a*-GFP<sup>+</sup> cells) in the brain, middle trunk, and tail at 4 dpf. The RBI-derived cells (top) were found in brain (dorsal view, rostral to the left, midbrain region), middle trunk, and tail (blue and orange boxed regions shown in [Figure 1B](#)), whereas the VDA-region-derived (middle) and PBI-derived (bottom) cells were detected in the trunk and tail but rarely in the brain. White arrows indicate GFP<sup>+</sup> cells.

(C) Quantification of GFP<sup>+</sup> cells derived from the RBI (n = 9), VDA region (n = 10), or PBI (n = 6) in the brain. Error bars represent mean ± SEM. \*\*\*p < 0.001.

(D) Quantification of GFP<sup>+</sup> cells derived from the RBI (n = 6), VDA region (n = 6), or PBI (n = 6) in the middle trunk. Error bars represent mean ± SEM. \*p < 0.05.

(E) Quantification of GFP<sup>+</sup> cells derived from the RBI (n = 6), VDA region (n = 6), or PBI (n = 6) in the tail. Error bars represent mean ± SEM. \*p < 0.05; \*\*\*p < 0.001.

See also [Figure S1](#).

VDA-region-derived cells because of the lack of circulation. At 2–3 hr after laser-mediated heat shock treatment, the embryos were fixed and subjected to whole-mount in situ hybridization (WISH) with anti-sense *CreER<sup>T2</sup>* probe. As shown in [Figure 2A](#), the infrared laser irradiation induced a robust *CreER<sup>T2</sup>* expression specifically in the targeted regions ([Figures 2A](#) and [S1A](#)). More importantly, this infrared laser-evoked *CreER<sup>T2</sup>* expression was sufficient to mediate *loxP* excision as indicated by the appearance of GFP-positive (GFP<sup>+</sup>) cells 1 day after the heat-shocked embryos were treated with the 4-OHT ([Figure S1B](#)). GFP<sup>+</sup> cells can be observed throughout the body of RBI-labeled embryos, whereas they only start to emerge in the middle and posterior parts of body in VDA-region-labeled and PBI-labeled embryos ([Figure S1B](#)). By 4 dpf, each group of the labeled embryos exhibited a unique GFP<sup>+</sup> distribution pattern ([Figures 2B–2E](#)): GFP<sup>+</sup> cells in the RBI-labeled embryo were found more abundantly in the brain and tail, GFP<sup>+</sup> cells in the VDA-region-labeled embryos were detected mainly in the trunk and tail, and GFP<sup>+</sup> cells in the PBI-labeled embryos were restricted to the tail ([Figures 2B–2E](#)). These results show that the IR-LEGO-CreER-loxP system indeed provides a temporal-spatial cell labeling with high resolution.

### Microglia in the Larval and Adult CNS Arise from Distinctive Origins

To determine the developmental timing and origin of microglia during CNS development and adult CNS homeostasis, we applied this temporal-spatial restricted IR-LEGO-CreER-loxP system to specifically label the RBI, VDA, and PBI regions of *Tg(hsp70:mCherry-T2a-CreER<sup>T2</sup>;**coro1a:loxP-DsRedx-loxP-GFP)* embryos. The contribution of each of these regions to

microglia in the brain and spinal cord was determined at 4 dpf (early larva), 15 dpf (late larva), 1.5 months (juvenile), 3 months (young adult), and 1 year (older adult) by quantifying the percentage of GFP<sup>+</sup> cells in total microglia by immunohistochemistry ([Figure 3](#)). Using Lcp1 as a microglia marker ([Herbomel et al., 1999; Li et al., 2012a; Meijer et al., 2008](#)), a significant number of GFP and Lcp1 double positive (GFP<sup>+</sup>/Lcp1<sup>+</sup>) microglia (on average ~43%) were detected in the brains of 4 dpf RBI-labeled embryos by immunohistochemistry, whereas GFP<sup>+</sup> cells were rarely seen in the brains of 4 dpf VDA-region-labeled and PBI-labeled embryos ([Figures 3B](#) and [3D](#)). These data demonstrate that at early larva stage the brain microglia are derived from the RBI. This result is in agreement with the previous findings showing that murine microglia arise from the YS ([Ginhoux et al., 2010; Schulz et al., 2012](#)). Surprisingly, when we examined the juvenile and adult fish, we found that the contribution of RBI-derived microglia in the brain declined dramatically and eventually became undetectable by the age of 1 year old ([Figures 3C](#) and [3D](#)), suggesting that the microglia in adult zebrafish brain might be derived from other source. Indeed, we observed that the VDA-region-derived microglia began to populate the brain from 15 dpf onward and their numbers increased rapidly as fish grew and eventually became the dominant population in 3-month-old young adult fish (~46% GFP<sup>+</sup> in the VDA region-labeling fish versus ~3% GFP<sup>+</sup> in the RBI-labeled fish) ([Figures 3C](#) and [3D](#)). We also labeled either anterior or posterior half of the VDA region and found that both parts could generate large number of microglia at about 25 dpf, suggesting that microglia progenitors spread along the VDA region (data not shown). In contrast to the early colonization of the brain, microglia populated the spinal cord

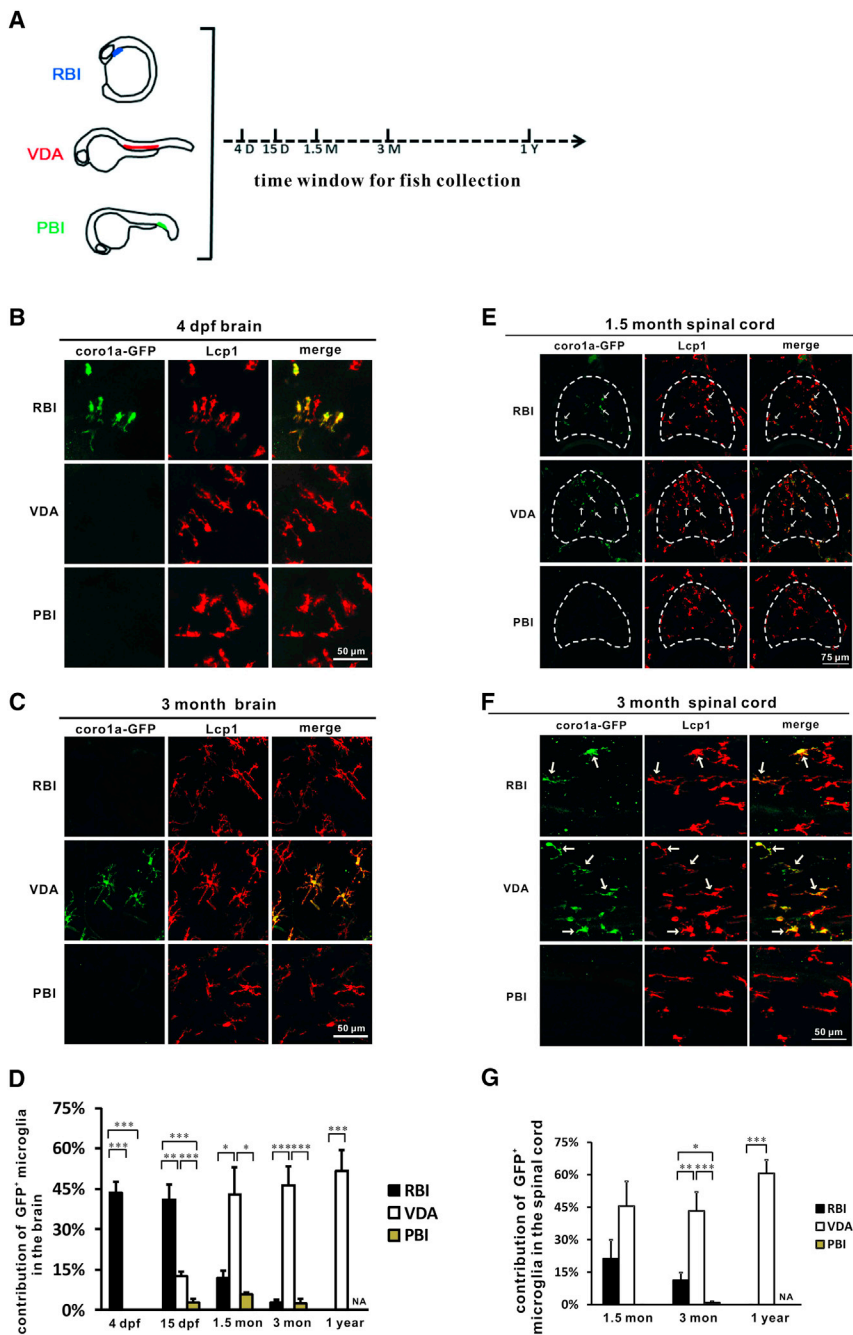


**Figure 3. Embryonic/Larval and Adult Microglia in Zebrafish CNS Arise from Distinct Origins**

(A) A timeline shows the experimental setup. The RBI-, VDA-, and PBI-region-labeled fish were raised and collected at 4 dpf, 15 dpf, 1.5 months, 3 months, and 1 year for analysis.

(B) Immunohistochemistry showed that the RBI-but not VDA- and PBI-region-derived cells (coro1a-GFP+ cells) constitute the major population of microglia (Lcp1+ cells) in the brains of 4-dpf zebrafish (dorsal view, rostral to the left, a part of the optic tectum).

(C) Immunohistochemistry showed that the VDA-but not RBI- and PBI-derived cells (coro1a-GFP+ cells) constitute the major population of microglia (Lcp1+ cells) in the brains of 3-month-old adult zebrafish (sectioned brain).

(D) Quantification of the contribution of the RBI-, VDA-, and PBI-region -derived microglia in the developing and adult zebrafish brain. For the RBI-labeled 4-dpf, 15-dpf, 1.5-month, 3-month, and 1-year adult fish, n = 8, 8, 5, 8, and 10, respectively; for the VDA-region-labeled 4-dpf, 15-dpf, 1.5-month, 3-month, and 1-year adult fish, n = 5, 6, 5, 8, and 9, respectively; for the PBI-labeled 4-dpf, 15-dpf, 1.5-month, and 3-month adult fish, n = 7, 6, 7, and 8 respectively. Error bars represent mean ± SEM. \*p < 0.05; \*\*p < 0.01; \*\*\*p < 0.001.

(E) Immunohistochemistry showed the contribution of the RBI-, VDA-, and PBI-region-derived cells (coro1a-GFP+ cells) to microglia (Lcp1+ cells) in the sectioned 1.5-month zebrafish spinal cord (indicated by the dashed lines). White arrows indicate the coro1a-GFP+ microglia in the spinal cord.

(F) Immunohistochemistry showed the contribution of the RBI-, VDA-, and PBI-region-derived cells (coro1a-GFP+ cells) to microglia (Lcp1+ cells) in the whole-mount 3-month adult zebrafish spinal cord. White arrows indicate the coro1a-GFP+ microglia in the spinal cord.

(G) Quantification of the contribution of RBI-, VDA-, and PBI-region-derived microglia in 1.5-month, 3-month, and 1-year adult zebrafish spinal cord. For the RBI-labeled 1.5-month, 3-month, and 1-year adult fish, n = 6, 12, and 8, respectively; for the VDA-region-labeled 1.5-month, 3-month, and 1-year adult fish, n = 4, 5, and 9, respectively; for the PBI-labeled 1.5-month and 3-month adult fish, n = 5 and 6, respectively. Error bars represent mean ± SEM. \*p < 0.05; \*\*p < 0.01; \*\*\*p < 0.001. See also [Figure S2](#).

between 15 dpf and 1.5 months ([Figure S2](#)). Similar to the brain, both RBI- and VDA-region-derived microglia could be observed in 1.5-month spinal cord, and as fish grew up, the VDA-region-derived microglia became the primary population in the spinal cord ([Figures 3E–3G](#)). Unlike the RBI and VDA, the PBI contributed very few cells to brain and spinal cord microglia throughout the development and adulthood of zebrafish ([Figures 3B–3G](#)). Collectively, these lineage tracing data indicate that the embryonic/larval and adult microglia in the zebrafish CNS are derived from two distinct sources: the RBI and the VDA regions, respectively.

**Microglia in the Retina Are Derived from Multiple Origins and Manifest a Different Temporal Distribution from Those in the CNS**

Because retina is also known to be colonized by microglia, we next investigated whether the retina microglia shared the same developmental origins and colonization time windows as those in the CNS. Results showed that similar to those in the brain, microglia populating the retina at 4 dpf were from the RBI region, whereas the VDA-region-derived cells began to colonize retina at 15 dpf ([Figures 4A and 4C](#)). Interestingly, in contrast to the brain where the RBI region-derived microglia declined

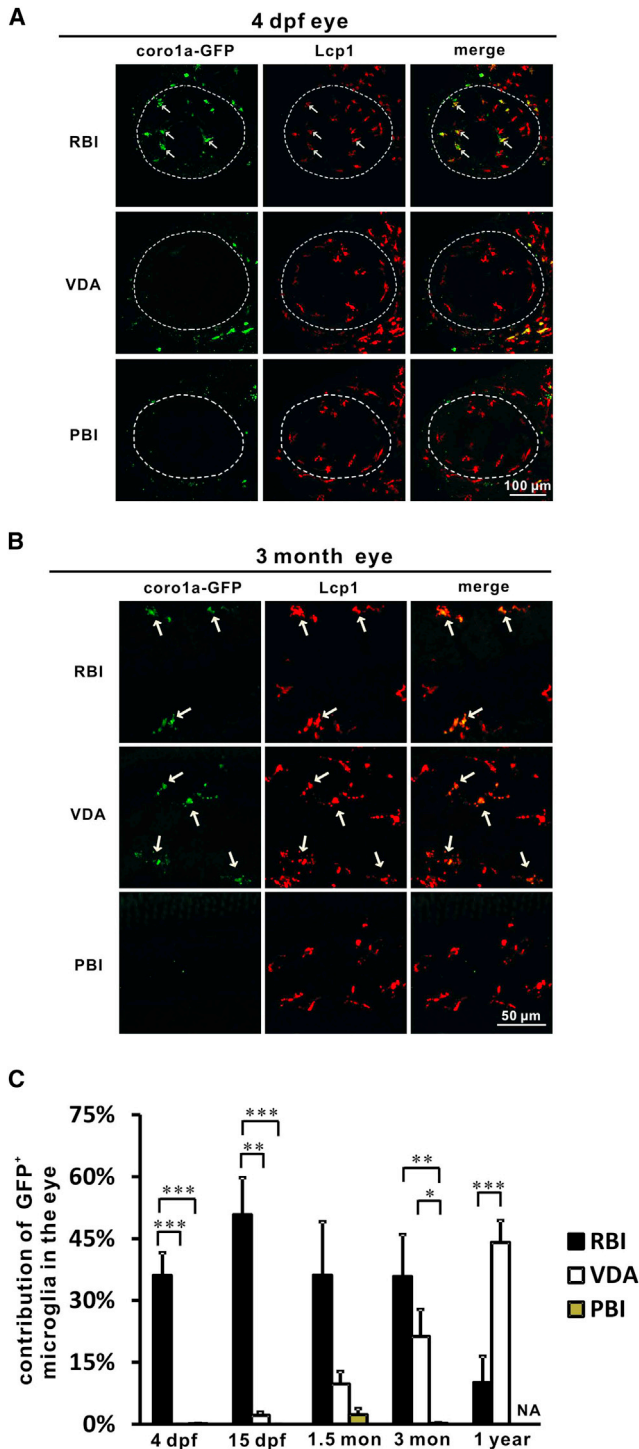


**Figure 4. The Microglia in the Eye Exhibit Distinct Colonization and Composition Profile to the Microglia in the CNS**

(A) The RBI- but not VDA- and PBI-region-derived cells (*coro1a*-GFP<sup>+</sup> cells) constitute the major population of microglia (Lcp1<sup>+</sup> cells) in the eyes (indicated by dashed lines) of 4-dpf zebrafish. White arrows indicate *coro1a*-GFP<sup>+</sup> microglia in the eyes.

(B) The RBI- and VDA- but not PBI-region-derived cells (*coro1a*-GFP<sup>+</sup> cells) constitute the major population of microglia (Lcp1<sup>+</sup> cells) in the 3-month adult zebrafish eye. White arrows indicate the *coro1a*-GFP<sup>+</sup> microglia in the eyes.

dramatically from juvenile stage onward and eventually became undetectable in adulthood (Figures 3B, 3C, 3E, and 3F), a significant portion (36% on average) of the RBI region-labeled microglia remained in the retina of 3-month-old young adult fish (Figures 4B and 4C). When the fish were 1 year old, the RBI-labeled microglia declined dramatically (~10% on average was left in the retina) and the VDA-region-derived microglia became the dominant population (~44% on average in the retina) (Figure 4C). These data suggest that the RBI region-derived microglia in the retina sustain much longer than those in the brain and spinal cord. Again, very few PBI region-derived microglia were found in the retina throughout development and adulthood of zebrafish (Figures 4A–4C). Taken together, these results demonstrate that the retina microglia are also derived from two separated origins, the RBI and VDA regions.

### Pu.1 Is Differentially Required for the RBI- and VDA-Region-Derived Microglia

Previous study has indicated that the development of microglia in mice requires Pu.1 (Kierdorf et al., 2013), an Ets transcription factor essential for myeloid lineage development (McKercher et al., 1996; Scott et al., 1994). We therefore sought to investigate whether the development of both RBI- and VDA-region-derived populations requires Pu.1. To address this question, we monitored the number of microglia in the hypomorphic *pu.1*<sup>G242D</sup> mutant fish, in which the G<sub>242</sub> to D mutation leads to a marked decrease of Pu.1 protein (Jin et al., 2012). Consistent with previous findings (Jin et al., 2012; Peri and Nüsslein-Volhard, 2008), attenuation of Pu.1 function in zebrafish severely impaired microglia development shown by the marked reduction of Lcp1 staining in the brains of 3 and 4 dpf *pu.1*<sup>G242D</sup> mutants (Figures 4A and 4B). Intriguingly, Lcp1<sup>+</sup> microglia began to recover in the mutant brain from 5 dpf onward, and by 6 dpf, the number of Lcp1<sup>+</sup> microglia in *pu.1*<sup>G242D</sup> mutant brain were comparable to that in WT (Figures 5A and 5B). Similar to the case in the brain, the microglia in the eye were also largely depleted at early stages but gradually recovered later (data not shown). Given the fact that the RBI-derived microglia initiate early and the VDA-region-born population emerges later, it is likely that the RBI-derived microglia are depleted in *pu.1*<sup>G242D</sup> mutants but the VDA-region-derived ones are not affected. To test this possibility, we used the IR-LEGO-CreER-*loxP* system to label the RBI and VDA regions of *pu.1*<sup>G242D</sup> mutants and the result showed that the recovered microglia in the brains of 8 dpf *pu.1*<sup>G242D</sup> mutants were indeed derived from the VDA region (~45.7% GFP<sup>+</sup> microglia in the VDA-region-labeled embryos) but not the RBI (0% GFP<sup>+</sup> microglia in the RBI-labeled embryos) (Figures 5C and 5D). In contrast, very few (~0.9%) microglia were derived from the VDA region in 8 dpf WT embryos (data not shown). Likewise, the recovered microglia in the retina of 8 dpf *pu.1*<sup>G242D</sup> mutants were also mainly derived from the VDA region (data not shown).

(C) Quantification of the contribution of the RBI-, VDA-, and PBI-region-derived microglia in the developing and adult zebrafish eyes. For the RBI-labeled 4-dpf, 15-dpf, 1.5-month, 3-month, and 1-year adult fish, n = 8, 8, 5, 8, and 10, respectively; for the VDA-region-labeled 4-dpf, 15-dpf, 1.5-month, 3-month, and 1-year adult fish, n = 5, 6, 5, 8, and 9, respectively; for the PBI-labeled 4-dpf, 15-dpf, 1.5-month, and 3-month adult fish, n = 7, 6, 7, and 8, respectively. Error bars represent mean ± SEM. \*p < 0.05; \*\*p < 0.01; \*\*\*p < 0.001.

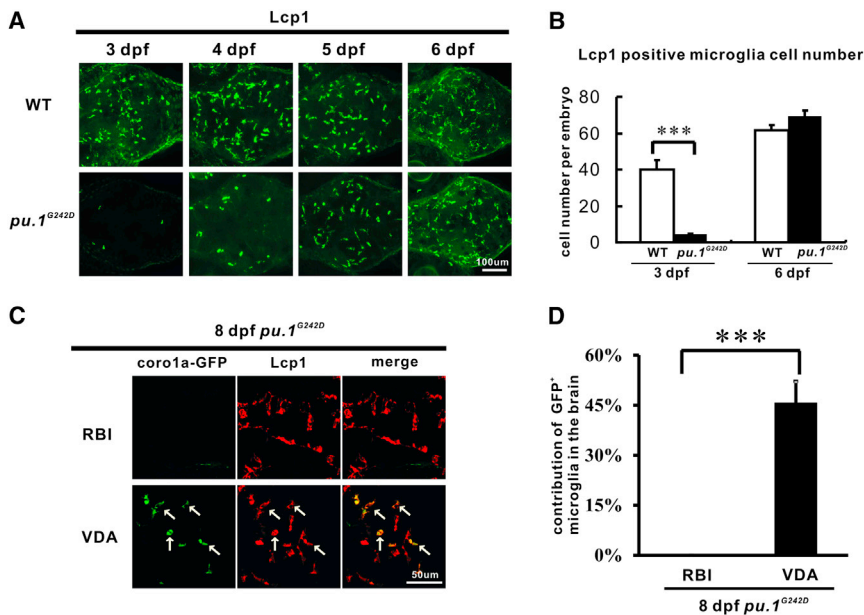


**Figure 5. The RBI- but not VDA-Region-Derived Microglia Are Depleted in *pu.1<sup>G242D</sup>* Mutants**

(A) Microglia are largely absent in *pu.1<sup>G242D</sup>* mutants at 3 dpf, but are fully recovered at 6 dpf. Stacked confocal images of immunohistochemistry staining of Lcp1 of 3-dpf, 4-dpf, 5-dpf, and 6-dpf WT and *pu.1<sup>G242D</sup>* embryos from the dorsal view of the brain shows the recovery of microglia in *pu.1<sup>G242D</sup>* mutants from 5 dpf onward.

(B) Quantification of Lcp1<sup>+</sup> microglia number in WT (n = 6) and *pu.1<sup>G242D</sup>* embryos (n = 6) at 3 dpf and 6 dpf. Error bars represent mean ± SEM. \*\*\*p < 0.001.

(C) Coro1a-GFP<sup>+</sup> microglia are observed in VDA- but not RBI-region-labeled *pu.1<sup>G242D</sup>* embryos at 8 dpf. White arrows indicate the coro1a-GFP<sup>+</sup> microglia in the brain (dorsal view, rostral to the left, a part of the optic tectum).

(D) Quantification of the contribution of RBI- and VDA-region-derived microglia in 8 dpf *pu.1<sup>G242D</sup>* embryos. For the RBI- and VDA-region-labeled embryos, n = 3 and 6, respectively. Error bars represent mean ± SEM. \*\*\*p < 0.001.

Taken together, these results indicate that the VDA-region-born microglia are differentially regulated from those derived from the RBI.

### The Development of the VDA Region-Derived Microglia Is *cMyb* Independent but *Runx1* Dependent

The above fate-mapping analysis indicates that the adult microglia are derived from the VDA region in zebrafish, a hematopoietic tissue equivalent to mouse AGM where HSCs are born (Bertrand et al., 2010; Kissa and Herbomel, 2010). We next sought to determine whether the generation of the VDA region-derived microglia was dependent on the differentiation of HSCs. To answer this question, we examined the formation and colonization of the VDA-region-derived microglia in the brain of zebrafish *cmyb<sup>hkz3</sup>* mutants, in which HSCs are gradually depleted because of the delay of migrating away from the VDA region and proliferation/differentiation in the VDA and CHT regions, due to the inactivation of *cMyb*, a transcription factor essential for HSC development in mice and fish (Mucenski et al., 1991; Mukouyama et al., 1999; Soza-Ried et al., 2010; Sumner et al., 2000; Zhang et al., 2011). Because *cmyb<sup>hkz3</sup>* mutants cannot survive beyond one month old, we examined the brain microglia at 20 dpf, a time when a substantial number of the VDA-region-derived microglia are present in wild-type (WT) larvae (Figures 6A and 6B). Results showed that a significant portion (on average 14.3%) of the VDA-region-derived microglia were present in the brains of 20 dpf *cmyb<sup>hkz3</sup>* mutants (Figures 6A and 6B), whereas T lymphocytes and erythrocytes were largely absent (Figures S3C and S3D). It is likely that the slightly lower contribution in the mutants (14.3% in *cmyb<sup>hkz3</sup>* mutants versus 22.3% in WT) (Figure 6B) was due to the developmental delay of the *cmyb<sup>hkz3</sup>* mutants as the average body length of 20 dpf mutant larvae (5.6 mm) was significantly smaller than that of 20 dpf control WT (7.2 mm) (Figures S3A and S3B). Indeed, a comparable number of the VDA-region-derived microglia were found in the brains of 20 dpf *cmyb<sup>hkz3</sup>* mutants and

15 dpf WT larvae (14.3% in *cmyb<sup>hkz3</sup>* mutants versus 12.6% in WT) (Figure 6B) with similar body length (5.6 mm in *cmyb<sup>hkz3</sup>* mutants versus 5.5 mm in WT) (Figure S3B). These results indicate that the development of the VDA-region-derived microglia is independent of *cMyb*, implying that the VDA-region-derived microglia may originate from the VDA-born precursors distinct from HSCs. It is well known that the hematopoietic cells in the VDA region are generated via the endothelial hematopoietic transition (EHT) in a *Runx1*-dependent fashion (Bertrand et al., 2010; Boisset et al., 2010; Chen et al., 2009; Kissa and Herbomel, 2010). We therefore reasoned that the VDA-region-derived microglia are *Runx1*-dependent, if they are indeed generated from the VDA. To test this notion, we examined microglia in *pu.1<sup>G242D</sup>runx1<sup>W84X</sup>* double mutants and *pu.1<sup>G242D</sup>* and *runx1<sup>W84X</sup>* single mutants. As expected, abundant microglia were present in both single mutants at 6 dpf because *Runx1* is known to be dispensable for the RBI-derived microglia development and the VDA-derived microglia has already colonized the *pu.1<sup>G242D</sup>* brains by 6 dpf (Figure 6C) (Jin et al., 2012). However, microglia were completely absent in *pu.1<sup>G242D</sup>runx1<sup>W84X</sup>* double mutants (Figure 6C), showing that the recovered microglia derived from the VDA region are abolished in the double mutants. This result supports the notion that the VDA-region-derived microglia are indeed derived from the VDA.

### DISCUSSION

In this study, we unambiguously document that in zebrafish the embryonic/larval and adult microglia arise from two distinct sources: embryonic/larval microglia originates from the RBI, a tissue analogous to mouse YS, whereas adult microglia arises from the VDA region. This result is different from previous findings indicating that microglia in mice are derived from a single origin, the mouse YS (Ginhoux et al., 2010; Ginhoux and Jung, 2014; Gomez Perdiguero et al., 2015; Hashimoto et al., 2013; Hoeffel et al., 2015; Kierdorf et al., 2013; Perdiguero et al.,

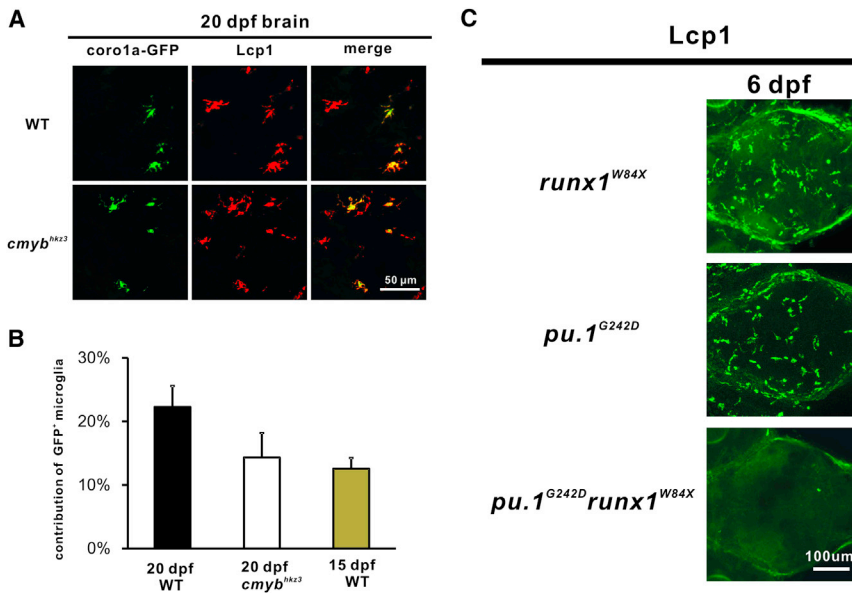


**Figure 6. The Development of VDA Region-Derived Microglia Is Independent of cMyb but Requires Runx1**

(A) The VDA-region-derived *coro1a*-GFP<sup>+</sup> cells contribute to brain microglia in 20 dpf WT and *cmyb<sup>hkz3</sup>* mutant embryos (sectioned brain). (B) Quantification of the contribution of the VDA-region-derived brain microglia in 20-dpf WT (n = 8), *cmyb<sup>hkz3</sup>* mutant (n = 8), and 15-dpf WT larvae (n = 6). Error bars represent mean ± SEM. (C) Microglia fail to recover in the *pu.1<sup>G242D</sup>runx1<sup>W84X</sup>* double mutants at 6 dpf. Stacked confocal images of immunohistochemistry staining of Lcp1 of 6 dpf *runx1<sup>W84X</sup>*, *pu.1<sup>G242D</sup>* single mutants, and *pu.1<sup>G242D</sup>runx1<sup>W84X</sup>* double mutant from the dorsal view of the brain. See also Figure S3.

ment of microglia in adult mice is also independent of cMYB (Schulz et al., 2012). It is therefore possible that adult microglia in mice might be derived from the AGM-

2014; Schulz et al., 2012). This discrepancy could be simply due to the species variations between mice and fish. However, given the fact that the hematopoietic program in zebrafish and mammals is highly conserved, it is possible that, in addition to the YS, the AGM and perhaps other regions in mice are also capable of contributing to the microglia pool and that these regions have not been identified because of insufficient temporal-spatial resolution of traditional CreER-*loxP* labeling methods used in previous studies. Another possibility is that there are multiple distinct sources of hematopoietic cells in the mouse YS as indicated by previous studies (Bertrand et al., 2005b; Hoeffel et al., 2015; McGrath et al., 2015), which give rise to embryonic and adult microglia, respectively. It is therefore of great interest to re-investigate the origin(s) of microglia in mice by using a high temporal-spatial resolution approach.

Our results demonstrate that the development of the VDA-region-derived microglia required Runx1 but is independent of cMyb, two transcription factors essential for HSC development at different stages in mice and fish (Chen et al., 2009; Kissa and Herbolme, 2010; Mucenski et al., 1991; Mukoyama et al., 1999; Soza-Ried et al., 2010; Sumner et al., 2000; Zhang et al., 2011). Two possible mechanisms may explain these interesting observations. One possibility is that adult microglia in the *cmyb*-deficient mutants are derived from the VDA-region-born HSCs, which are capable of differentiating into microglia even though they fail to leave the VDA region and are gradually depleted. Alternatively, the development of adult microglia in zebrafish may be independent of HSCs, which implies that in addition to producing HSCs (Burns et al., 2005; Gering and Patient, 2005), the VDA region may also generate a distinct population of hematopoietic precursors capable of giving rise to adult microglia. In line with this notion, several previous studies in mice and chicks have suggested that the hematopoietic cells born in the AGM are not homogenous because these AGM-born cells appear to manifest distinct differentiation potential (Bertrand et al., 2005a; North et al., 2002; Ody et al., 1999; Taoudi and Medvinsky, 2007; Yoshimoto et al., 2011). Interestingly, the develop-

ment of microglia in adult mice is also independent of cMYB (Schulz et al., 2012). It is therefore possible that adult microglia in mice might be derived from the AGM-

born precursors distinctive from conventional HSCs. Further in-depth study is required to clarify these two possibilities. Another interesting observation is that Pu.1 is differentially required for the development of the RBI and VDA-region-derived microglia. This result is different from the previous findings showing that the microglia are absent in the brains of 14-day post conception (dpc) Pu.1 knockout mice (Kierdorf et al., 2013). One possible explanation of this discrepancy is that the low Pu.1 activity in *pu.1<sup>G242D</sup>* hypomorphic allele mutants is sufficient for the development of the VDA region-derived microglia. It would be of great interest to create a *pu.1* null allele to further investigate the role of Pu.1 in zebrafish microglia development. Another explanation of the discrepancy is that the microglia in the brain of 14 dpc mouse embryos, the stage where microglia are examined in previous studies in mice (Kierdorf et al., 2013), may represent primitive microglia equivalent to the embryonic microglia in zebrafish, which are Pu.1-dependent. Notably, in *pu.1<sup>G242D</sup>* mutants, the VDA-region-derived microglia colonize the brain earlier than that in WT. The precise mechanism underlying this early brain colonization is not fully understood. We speculate that the depletion of RBI-derived microglia may lead to the accumulation of chemotactic cues (perhaps also provides anatomical spaces) in the brain, which could promote early colonization of the mutant brain by the VDA region-derived microglia. All these issues warrant further investigation.

A remarkable distinct feature of the RBI- and VDA-region-derived microglia is their long-term CNS colonization potential. Whereas the colonization of the CNS by the RBI-derived microglia is limited to larval and juvenile stages, the microglia derived from the VDA region appear to be the exclusive population with long-term colonization potential (Figure 7). The distinctive CNS colonization potential is likely ascribed to the differences in their intrinsic genetic program because neither the RBI-derived nor VDA-region-derived microglia display unique colonization pattern in the CNS. The intrinsic genetic program difference is supported by our finding that the RBI- and VDA-region-derived microglia have distinct requirements for Pu.1 activity,

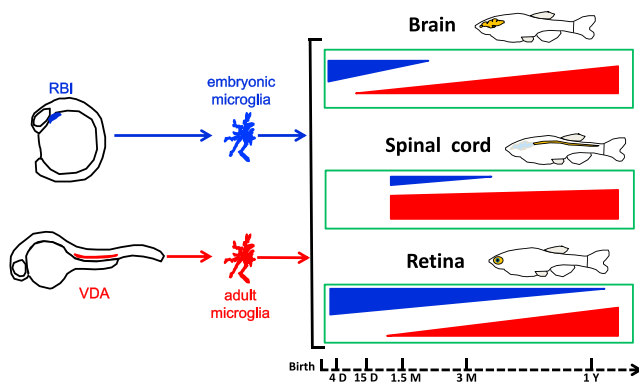


**Figure 7. Summary of Microglia Generation in Zebrafish**

Microglia in developing and adult zebrafish are generated from two distinct origins. The embryonic/larval microglia arise from the RBI, and they colonize the CNS and retina temporally with distinct sustainability in the brain, spinal cord, and retina. On the other hand, the adult microglia are derived from the VDA region and they are the exclusive microglia population capable of long-term colonization of the CNS and retina.

an essential transcription factor for myeloid cell development (McKercher et al., 1996; Scott et al., 1994). The precise molecular basis underlying the unique features of the two different populations of microglia remains unknown. A comprehensive comparison of gene expression profile of the RBI- and VDA-region-derived microglia will provide clues to answer this question. Interestingly, although lack of long-term colonization potential, the RBI-derived microglia exhibit distinct sustainability in the CNS and retina, suggesting that the micro-environment also influences the colonization potential of microglia. This finding is consistent with the recent studies showing that in mice the local tissue micro-environment has a significant impact on shaping the identity and plasticity of tissue-resident macrophages (Gosselin et al., 2014; Lavin et al., 2014). Because adult microglia are believed to be capable of self-replenishment throughout development and adult life (Ajami et al., 2007; Ginhoux et al., 2010; Mildner et al., 2007), it will be interesting to find out whether the renewal potential of microglia or microglia stem cells, if they exist, requires a specific micro-environment.

The distinctive temporal-spatial distribution in the brain, spinal cord, and retina by the RBI- and VDA-derived microglia suggests that they may manifest diverse biological functions in developing and adult zebrafish in a non-redundant manner. Our preliminary data suggest that the depletion of the RBI-derived microglia could lead to delayed removal of apoptotic neurons, vacuole formation, and reduced spontaneous neuronal activity, suggesting that the RBI-derived microglia play an essential role during early neurogenesis that cannot be fully compensated by the VDA-derived population (unpublished data). Further in-depth studies to uncover the functions of the two distinct microglia populations in zebrafish will significantly enhance our understanding of the roles of microglia in the developing and adult CNS.

## EXPERIMENTAL PROCEDURES

### Zebrafish

Zebrafish were maintained according to standard protocol (Westerfield, 1995). AB wild-type, *cmlyb*<sup>hkc3</sup> mutant (Zhang et al., 2011), *pu.1*<sup>G242D</sup> (Jin et al., 2012),

*runx1*<sup>W84X</sup> (Jin et al., 2009; Sood et al., 2010), *Tg(hsp70:mCherry-T2a-CreER*<sup>T2</sup><sup>#12</sup>) (Hans et al., 2011), and *Tg(coro1a:loxP-DsRedx-loxP-GFP)hkztg12* lines were used in this study.

### The IR-LEGO-CreER-loxP System and Cell Labeling

To generate the 1,345 nm infrared laser, a femtosecond Ti:sapphire laser (Chameleon Ultra II, Coherent) was tuned at 830 nm to pump an optical parametric oscillator (Chameleon OPO, Coherent) to emit infrared beam with a wavelength of 1,345 nm. The 1,345 nm laser was focused on zebrafish mounted in methylcellulose by a coated achromatic doublet lens (AC254-060-B, Thorlabs, focal length: 60 mm). The LED light source is placed beneath the zebrafish and illuminates the sample through a condenser (U-AAC, Achromat/aplanat condenser, NA 1.4, Olympus). The zebrafish is imaged on the CCD camera with 140× magnification to identify the cell regions for heat-shock gene induction. The power of 1,345 nm on the sample surface was ~65–80 mW and the duration of each localized heat shock was 2 min. The RBI was heat-shocked by irradiating three positions along the RBI region from one side of zebrafish at 12–16 hpf. The PBI labeling was performed by irradiating two positions along the PBI region at ~20–22 hpf. The VDA region labeling was performed by irradiating four positions along the VDA region at 28–30 hpf. Immediately after irradiation, the embryos were treated with 4-OHT for 17–22 hr. The efficiency of cell labeling was determined under fluorescent microscope 1 day and 3 days after heat shock. The fish with significant GFP contribution was selected and raised for further analysis.

### Generation of Transgenic Lines

The promoter of *coro1a* gene, *loxP* sequence, coding regions of *DsRedx* and *GFP* were cloned into the pTol2 vector to generate the *coro1a:loxP-DsRedx-loxP-GFP* and *coro1a:DsRedx* constructs. The resulting construct was injected, together with the mRNA of transposase, into one-cell stage fertilized embryos (Kawakami et al., 2000).

### Whole-Mount In Situ Hybridization

Antisense DIG-labeled *Cre* and *rag1* RNA probe was synthesized in vitro. The embryos at desired stages were fixed by 4% PFA. Standard protocol was performed to detect signal (Westerfield, 1995).

### Fish Dissection, Antibody Staining, and Imaging

All the samples were directly fixed in 4% PFA at 4°C for 1–2 days. After washing with PBS at 4°C for 1–3 days, the fish were either directly subjected to whole-mount antibody staining (4 dpf and 15 dpf fish) or dissection (1.5 month and adult fish). Fifteen-dpf fish were further sectioned after antibody staining for imaging. The spinal cords in adult fish were dissected and directly apply to whole-mount antibody staining; whereas the brains and eyes were applied to cryo-section followed by antibody staining. Whole-mount antibody staining was carried out as described elsewhere (Barresi et al., 2000; Jin et al., 2006) and cryo-section was performed at 30-μm intervals in transverse planes and immunohistochemistry was performed as previously described (Wendl et al., 2002). All images were captured by Leica SP8 confocal microscope and the quantification was done manually. The primary antibodies used in this study included Anti-GFP antibody (ab6658, Abcam), anti-Lcp1 antibody (Jin et al., 2009), and anti-hemoglobin  $\alpha$ e1 (Jin et al., 2007). The secondary antibodies used in this study were Alexa 488-anti-goat antibody (A11055 Invitrogen), Alexa 555-anti-rabbit antibody (A31572 Invitrogen), and Alexa 647-anti-rabbit antibody (A31573 Invitrogen).

### Mutant Identification

*pu.1*<sup>G242D</sup> mutants were genotyped by PCR followed by BsmFI digestion. The mutant PCR products were digested by BsmFI into two fragments of 127 bp and 117 bp, respectively, whereas WT PCR products were resistant to the BsmFI digestion. Primers for *pu.1*<sup>G242D</sup> genotyping: 5'-CTGCTTGACCTTCTGCGAAA-3'/5'-CCGAGAACCTCTCCACTGAA-3'.

### Statistical Analysis

The F-test of two-sample for variances, t test of two-sample assuming equal variances, and t test of two-sample assuming unequal variances were performed by the Data Analysis tool in the Excel software (Microsoft). Two-tailed p values are used for all t tests.

## SUPPLEMENTAL INFORMATION

Supplemental Information includes three figures and can be found with this article online at <http://dx.doi.org/10.1016/j.devcel.2015.08.018>.

## AUTHOR CONTRIBUTIONS

J.X., L.Z., S.C.H., Y.W., W.J., and T.Y. designed the research, performed experiments, and analyzed data. J.Y.Q. and Z.W. designed the research and analyzed data.

## ACKNOWLEDGMENTS

We thank Dr. Michael Brand for sharing the *Tg(hsp70:mCherry-T2a-CreER<sup>T2</sup>)* transgenic line; Dr. Koichi Kawakami for providing the pTol2 vector; and Tienan Wang, Li Li, Rui Zhuang, and Wei Fu for their technical assistance. We also thank Yan Yan, Tom Cheung, Mingjie Zhang, Hao Jin, and Nishanth Iyengar for critical reading of the manuscript. This work was supported by the National Natural Science Foundation of China (grant no. 31229003), the National Basic Research Program of China (grant no. 2012CB945102), and the Research Grants Council of the HKSAR (663212; HKUST6/CRF/09; HKUST5/CRF/12R; AoE/M-09/12; and T13-607/12R).

Received: April 28, 2015

Revised: July 5, 2015

Accepted: August 26, 2015

Published: September 28, 2015

## REFERENCES

- Ajami, B., Bennett, J.L., Krieger, C., Tetzlaff, W., and Rossi, F.M. (2007). Local self-renewal can sustain CNS microglia maintenance and function throughout adult life. *Nat. Neurosci.* **10**, 1538–1543.
- Barresi, M.J., Stickney, H.L., and Devoto, S.H. (2000). The zebrafish slow-muscle-omitted gene product is required for Hedgehog signal transduction and the development of slow muscle identity. *Development* **127**, 2189–2199.
- Bertrand, J.Y., Giroux, S., Golub, R., Klaine, M., Jalil, A., Boucontet, L., Godin, I., and Cumano, A. (2005a). Characterization of purified intraembryonic hematopoietic stem cells as a tool to define their site of origin. *Proc. Natl. Acad. Sci. USA* **102**, 134–139.
- Bertrand, J.Y., Jalil, A., Klaine, M., Jung, S., Cumano, A., and Godin, I. (2005b). Three pathways to mature macrophages in the early mouse yolk sac. *Blood* **106**, 3004–3011.
- Bertrand, J.Y., Kim, A.D., Violette, E.P., Stachura, D.L., Cisson, J.L., and Traver, D. (2007). Definitive hematopoiesis initiates through a committed erythromyeloid progenitor in the zebrafish embryo. *Development* **134**, 4147–4156.
- Bertrand, J.Y., Chi, N.C., Santoso, B., Teng, S., Stainier, D.Y., and Traver, D. (2010). Haematopoietic stem cells derive directly from aortic endothelium during development. *Nature* **464**, 108–111.
- Boisset, J.C., van Cappellen, W., Andrieu-Soler, C., Galjart, N., Dzierzak, E., and Robin, C. (2010). In vivo imaging of haematopoietic cells emerging from the mouse aortic endothelium. *Nature* **464**, 116–120.
- Burns, C.E., Traver, D., Mayhall, E., Shepard, J.L., and Zon, L.I. (2005). Hematopoietic stem cell fate is established by the Notch-Runx pathway. *Genes Dev.* **19**, 2331–2342.
- Chen, M.J., Yokomizo, T., Zeigler, B.M., Dzierzak, E., and Speck, N.A. (2009). Runx1 is required for the endothelial to hematopoietic cell transition but not thereafter. *Nature* **457**, 887–891.
- Ciau-Uitz, A., Monteiro, R., Kirmizitas, A., and Patient, R. (2014). Developmental hematopoiesis: ontogeny, genetic programming and conservation. *Exp. Hematol.* **42**, 669–683.
- Deguchi, T., Itoh, M., Urawa, H., Matsumoto, T., Nakayama, S., Kawasaki, T., Kitano, T., Oda, S., Mitani, H., Takahashi, T., et al. (2009). Infrared laser-mediated local gene induction in medaka, zebrafish and *Arabidopsis thaliana*. *Dev. Growth Differ.* **51**, 769–775.
- Epelman, S., Lavine, K.J., Beaudin, A.E., Sojka, D.K., Carrero, J.A., Calderon, B., Brija, T., Gautier, E.L., Ivanov, S., Satpathy, A.T., et al. (2014). Embryonic and adult-derived resident cardiac macrophages are maintained through distinct mechanisms at steady state and during inflammation. *Immunity* **40**, 91–104.
- Gekas, C., Dieterlen-Lièvre, F., Orkin, S.H., and Mikkola, H.K. (2005). The placenta is a niche for hematopoietic stem cells. *Dev. Cell* **8**, 365–375.
- Gering, M., and Patient, R. (2005). Hedgehog signaling is required for adult blood stem cell formation in zebrafish embryos. *Dev. Cell* **8**, 389–400.
- Ginhoux, F., and Jung, S. (2014). Monocytes and macrophages: developmental pathways and tissue homeostasis. *Nat. Rev. Immunol.* **14**, 392–404.
- Ginhoux, F., Greter, M., Leboeuf, M., Nandi, S., See, P., Gokhan, S., Mehler, M.F., Conway, S.J., Ng, L.G., Stanley, E.R., et al. (2010). Fate mapping analysis reveals that adult microglia derive from primitive macrophages. *Science* **330**, 841–845.
- Gomez Perdiguero, E., Klapproth, K., Schulz, C., Busch, K., Azzi, E., Crozet, L., Garner, H., Trouillet, C., de Bruijn, M.F., Geissmann, F., and Rodewald, H.R. (2015). Tissue-resident macrophages originate from yolk-sac-derived erythromyeloid progenitors. *Nature* **518**, 547–551.
- Gosselin, D., Link, V.M., Romanoski, C.E., Fonseca, G.J., Eichenfield, D.Z., Spann, N.J., Stender, J.D., Chun, H.B., Garner, H., Geissmann, F., and Glass, C.K. (2014). Environment drives selection and function of enhancers controlling tissue-specific macrophage identities. *Cell* **159**, 1327–1340.
- Hans, S., Freudenreich, D., Geffarth, M., Kaslin, J., Machate, A., and Brand, M. (2011). Generation of a non-leaky heat shock-inducible Cre line for conditional Cre/lox strategies in zebrafish. *Dev. Dyn.* **240**, 108–115.
- Hashimoto, D., Chow, A., Noizat, C., Teo, P., Beasley, M.B., Leboeuf, M., Becker, C.D., See, P., Price, J., Lucas, D., et al. (2013). Tissue-resident macrophages self-maintain locally throughout adult life with minimal contribution from circulating monocytes. *Immunity* **38**, 792–804.
- Herbomel, P., Thisse, B., and Thisse, C. (1999). Ontogeny and behaviour of early macrophages in the zebrafish embryo. *Development* **126**, 3735–3745.
- Hoeffel, G., Chen, J., Lavin, Y., Low, D., Almeida, F.F., See, P., Beaudin, A.E., Lum, J., Low, I., Forsberg, E.C., et al. (2015). C-Myb(+) erythro-myeloid progenitor-derived fetal monocytes give rise to adult tissue-resident macrophages. *Immunity* **42**, 665–678.
- Jagannathan-Bogdan, M., and Zon, L.I. (2013). Hematopoiesis. *Development* **140**, 2463–2467.
- Jin, H., Xu, J., Qian, F., Du, L., Tan, C.Y., Lin, Z., Peng, J., and Wen, Z. (2006). The 5' zebrafish scl promoter targets transcription to the brain, spinal cord, and hematopoietic and endothelial progenitors. *Dev. Dyn.* **235**, 60–67.
- Jin, H., Xu, J., and Wen, Z. (2007). Migratory path of definitive hematopoietic stem/progenitor cells during zebrafish development. *Blood* **109**, 5208–5214.
- Jin, H., Sood, R., Xu, J., Zhen, F., English, M.A., Liu, P.P., and Wen, Z. (2009). Definitive hematopoietic stem/progenitor cells manifest distinct differentiation output in the zebrafish VDA and PBl. *Development* **136**, 647–654.
- Jin, H., Li, L., Xu, J., Zhen, F., Zhu, L., Liu, P.P., Zhang, M., Zhang, W., and Wen, Z. (2012). Runx1 regulates embryonic myeloid fate choice in zebrafish through a negative feedback loop inhibiting Pu.1 expression. *Blood* **119**, 5239–5249.
- Jing, L., and Zon, L.I. (2011). Zebrafish as a model for normal and malignant hematopoiesis. *Dis. Model. Mech.* **4**, 433–438.
- Kamei, Y., Suzuki, M., Watanabe, K., Fujimori, K., Kawasaki, T., Deguchi, T., Yoneda, Y., Todo, T., Takagi, S., Funatsu, T., and Yuba, S. (2009). Infrared laser-mediated gene induction in targeted single cells in vivo. *Nat. Methods* **6**, 79–81.
- Kawakami, K., Shima, A., and Kawakami, N. (2000). Identification of a functional transposase of the Tol2 element, an Ac-like element from the Japanese medaka fish, and its transposition in the zebrafish germ lineage. *Proc. Natl. Acad. Sci. USA* **97**, 11403–11408.
- Kierdorf, K., Erny, D., Goldmann, T., Sander, V., Schulz, C., Perdiguero, E.G., Wieghofer, P., Heinrich, A., Riemke, P., Hölscher, C., et al. (2013). Microglia emerge from erythromyeloid precursors via Pu.1- and Irf8-dependent pathways. *Nat. Neurosci.* **16**, 273–280.

- Kissa, K., and Herbomel, P. (2010). Blood stem cells emerge from aortic endothelium by a novel type of cell transition. *Nature* *464*, 112–115.
- Kreutzberg, G.W. (1995). Microglia, the first line of defence in brain pathologies. *Arzneimittelforschung* *45* (3A), 357–360.
- Lavin, Y., Winter, D., Blecher-Gonen, R., David, E., Keren-Shaul, H., Merad, M., Jung, S., and Amit, I. (2014). Tissue-resident macrophage enhancer landscapes are shaped by the local microenvironment. *Cell* *159*, 1312–1326.
- Li, L., Yan, B., Shi, Y.Q., Zhang, W.Q., and Wen, Z.L. (2012a). Live imaging reveals differing roles of macrophages and neutrophils during zebrafish tail fin regeneration. *J. Biol. Chem.* *287*, 25353–25360.
- Li, Z., Lan, Y., He, W., Chen, D., Wang, J., Zhou, F., Wang, Y., Sun, H., Chen, X., Xu, C., et al. (2012b). Mouse embryonic head as a site for hematopoietic stem cell development. *Cell Stem Cell* *11*, 663–675.
- Lichanska, A.M., and Hume, D.A. (2000). Origins and functions of phagocytes in the embryo. *Exp. Hematol.* *28*, 601–611.
- Lin, Y., Yoder, M.C., and Yoshimoto, M. (2014). Lymphoid progenitor emergence in the murine embryo and yolk sac precedes stem cell detection. *Stem Cells Dev.* *23*, 1168–1177.
- McGrath, K.E., Frame, J.M., Fegan, K.H., Bowen, J.R., Conway, S.J., Catherman, S.C., Kingsley, P.D., Koniski, A.D., and Palis, J. (2015). Distinct Sources of Hematopoietic Progenitors Emerge before HSCs and Provide Functional Blood Cells in the Mammalian Embryo. *Cell Rep.* *11*, 1892–1904.
- McKercher, S.R., Torbett, B.E., Anderson, K.L., Henkel, G.W., Vestal, D.J., Baribault, H., Klemsz, M., Feeney, A.J., Wu, G.E., Paige, C.J., and Maki, R.A. (1996). Targeted disruption of the PU.1 gene results in multiple hematopoietic abnormalities. *EMBO J.* *15*, 5647–5658.
- Meijer, A.H., van der Sar, A.M., Cunha, C., Lamers, G.E., Laplante, M.A., Kikuta, H., Bitter, W., Becker, T.S., and Spaik, H.P. (2008). Identification and real-time imaging of a myc-expressing neutrophil population involved in inflammation and mycobacterial granuloma formation in zebrafish. *Dev. Comp. Immunol.* *32*, 36–49.
- Mildner, A., Schmidt, H., Nitsche, M., Merkler, D., Hanisch, U.K., Mack, M., Heikenwalder, M., Brück, W., Priller, J., and Prinz, M. (2007). Microglia in the adult brain arise from Ly-6ChiCCR2+ monocytes only under defined host conditions. *Nat. Neurosci.* *10*, 1544–1553.
- Mucenski, M.L., McLain, K., Kier, A.B., Swerdlow, S.H., Schreiner, C.M., Miller, T.A., Pietryga, D.W., Scott, W.J., Jr., and Potter, S.S. (1991). A functional c-myb gene is required for normal murine fetal hepatic hematopoiesis. *Cell* *65*, 677–689.
- Mukoyama, Ys., Chiba, N., Mucenski, M.L., Satake, M., Miyajima, A., Hara, T., and Watanabe, T. (1999). Hematopoietic cells in cultures of the murine embryonic aorta-gonad-mesonephros region are induced by c-Myb. *Curr. Biol.* *9*, 833–836.
- North, T.E., de Bruijn, M.F., Stacy, T., Talebian, L., Lind, E., Robin, C., Binder, M., Dzierzak, E., and Speck, N.A. (2002). Runx1 expression marks long-term repopulating hematopoietic stem cells in the midgestation mouse embryo. *Immunity* *16*, 661–672.
- Ody, C., Vaigot, P., Quéré, P., Imhof, B.A., and Corbel, C. (1999). Glycoprotein IIb-IIIa is expressed on avian multilineage hematopoietic progenitor cells. *Blood* *93*, 2898–2906.
- Orkin, S.H., and Zon, L.I. (2008). Hematopoiesis: an evolving paradigm for stem cell biology. *Cell* *132*, 631–644.
- Ottersbach, K., and Dzierzak, E. (2005). The murine placenta contains hematopoietic stem cells within the vascular labyrinth region. *Dev. Cell* *8*, 377–387.
- Perdiguer, E.G., Klapproth, K., Schulz, C., Busch, K., Azzoni, E., Crozet, L., Garner, H., Trouillet, C., de Bruijn, M.F., Geissmann, F., et al. (2014). Tissue-resident macrophages originate from yolk-sac-derived erythro-myeloid progenitors. *Nature*.
- Peri, F., and Nüsslein-Volhard, C. (2008). Live imaging of neuronal degradation by microglia reveals a role for v0-ATPase a1 in phagosomal fusion in vivo. *Cell* *133*, 916–927.
- Prinz, M., and Priller, J. (2014). Microglia and brain macrophages in the molecular age: from origin to neuropsychiatric disease. *Nat. Rev. Neurosci.* *15*, 300–312.
- Salter, M.W., and Beggs, S. (2014). Sublime microglia: expanding roles for the guardians of the CNS. *Cell* *158*, 15–24.
- Schulz, C., Gomez Perdiguer, E., Chorro, L., Szabo-Rogers, H., Cagnard, N., Kierdorf, K., Prinz, M., Wu, B., Jacobsen, S.E., Pollard, J.W., et al. (2012). A lineage of myeloid cells independent of Myb and hematopoietic stem cells. *Science* *336*, 86–90.
- Scott, E.W., Simon, M.C., Anastasi, J., and Singh, H. (1994). Requirement of transcription factor PU.1 in the development of multiple hematopoietic lineages. *Science* *265*, 1573–1577.
- Sood, R., English, M.A., Belele, C.L., Jin, H., Bishop, K., Haskins, R., McKinney, M.C., Chahal, J., Weinstein, B.M., Wen, Z., and Liu, P.P. (2010). Development of multilineage adult hematopoiesis in the zebrafish with a runx1 truncation mutation. *Blood* *115*, 2806–2809.
- Soza-Ried, C., Hess, I., Netuschil, N., Schorpp, M., and Boehm, T. (2010). Essential role of c-myb in definitive hematopoiesis is evolutionarily conserved. *Proc. Natl. Acad. Sci. USA* *107*, 17304–17308.
- Stachura, D.L., and Traver, D. (2011). Cellular dissection of zebrafish hematopoiesis. *Methods Cell Biol.* *101*, 75–110.
- Sumner, R., Crawford, A., Mucenski, M., and Frampton, J. (2000). Initiation of adult myelopoiesis can occur in the absence of c-Myb whereas subsequent development is strictly dependent on the transcription factor. *Oncogene* *19*, 3335–3342.
- Taoudi, S., and Medvinsky, A. (2007). Functional identification of the hematopoietic stem cell niche in the ventral domain of the embryonic dorsal aorta. *Proc. Natl. Acad. Sci. USA* *104*, 9399–9403.
- Wendl, T., Lun, K., Mione, M., Favor, J., Brand, M., Wilson, S.W., and Rohr, K.B. (2002). Pax2.1 is required for the development of thyroid follicles in zebrafish. *Development* *129*, 3751–3760.
- Westerfield, M. (1995). *The Zebrafish Book: A Guide for the Laboratory Use of Zebrafish (Danio rerio)*, Third Edition (Eugene, OR: University of Oregon Press).
- Xu, J., Du, L., and Wen, Z. (2012). Myelopoiesis during zebrafish early development. *J. Genet. Genomics* *39*, 435–442.
- Yoshimoto, M., Montecino-Rodriguez, E., Ferkowicz, M.J., Porayette, P., Shelley, W.C., Conway, S.J., Dorshkind, K., and Yoder, M.C. (2011). Embryonic day 9 yolk sac and intra-embryonic hemogenic endothelium independently generate a B-1 and marginal zone progenitor lacking B-2 potential. *Proc. Natl. Acad. Sci. USA* *108*, 1468–1473.
- Zhang, Y., Jin, H., Li, L., Qin, F.X., and Wen, Z. (2011). cMyb regulates hematopoietic stem/progenitor cell mobilization during zebrafish hematopoiesis. *Blood* *118*, 4093–4101.